

# Motif based high-throughput structure prediction of superconducting monolayer titanium boride

Jason Yu<sup>1\*</sup>    Jihai Liao<sup>1</sup>    Xiaobao Yang<sup>1</sup>    Yujun Zhao<sup>1</sup>    Yinchang Zhao<sup>2</sup>

<sup>1</sup>Department of Physics, South China University of Technology, Guangzhou 510640, People's Republic of China

<sup>2</sup> Department of Physics, Yantai University, Yantai 264005, P. R. China

## Abstract

Two-dimensional boron structures, due to the diversity of properties, attract great attention because of their potential applications in nanoelectronic devices. A series of  $\text{TiB}_x$  ( $4 \leq x \leq 11$ ) monolayers are efficiently constructed through our motif based method and theoretically investigated through high-throughput first-principles calculations. The configurations are generated based on motifs of boron triangular/quadrilateral fragments and multicoordinate titanium-centered boron molecular wheels. Besides previously reported  $\text{TiB}_4$  which was discovered by global search method, we predict that high symmetry monolayers  $\text{TiB}_7$  (Cmmm) and  $\text{TiB}_9$  (P31m) which are octa-coordinate and nona-coordinate titanium boride are thermodynamic stable. The  $\text{TiB}_7$  monolayer is a BCS superconductor with the transition temperature  $T_c$  up to 8K. The motif based approach is proved to be efficient in searching stable structures with a prior knowledge so that the potentially stable transition metal monolayers can be quickly constructed by using basic cluster motifs. As an efficient way of discovering materials, the method is easily extended to predict other type of materials which have common characteristic pattern in the structure.

## 1 Introduction

Boron demonstrates the structural diversity in low-dimensional systems due to the multicenter bonds, from zero-dimensional clusters to two-dimensional layers. The most stable  $\text{B}_{12}$  cluster is a fragment of planar triangular grids[42], which otherwise forms a highly symmetric icosahedron as bulk cluster[8]. As the size of clusters increases, the hexagonal vacancies were found to be energetically preferable[15, 24], such as  $\text{B}_{30}$  and  $\text{B}_{36}$ . Meanwhile, the stable boron monolayers with hexagonal vacancies were theoretically proposed[30, 40]. Various kinds of distributions of vacancies in borophene cause a variety of novel properties, including topological property[7], superconductivity[22, 48] and even forming the borophene semiconductor[36]. In the recent experiments[6, 19], boron monolayers were fabricated on the metallic substrates by the molecular beam epitaxy method, where the vacancy patterns could be neatly modulated by the type of substrate[33] and the growth conditions[47].

The structural diversity and corresponding properties of boron nanostructures were able to be further enhanced by nesting the metal atoms[16, 27, 28, 43, 44]. For instance, the band structure of quasi-monolayer  $\text{TiB}_2$  [44] was predicted to be characterized with anisotropic Dirac cones and the Fermi velocity of the material was as large as half of the graphene. As for the two-dimensional  $\text{MoB}_4$ [28], it revealed a novel electronic structure which contains double Dirac cones near Fermi level with high Fermi velocity and superconductivity with transition temperatures ( $T_c$ ) of 44.5K. Experimentally, various planar hyper-coordinate species of transition metal (TM)@ $\text{B}_n$  with transition metal atom locating at the center of the boron wheel were synthesised [27], which might serve as building blocks for the construction of transition metal boride monolayer.

Based on the first-principles calculations, the  $\text{FeB}_6$  monolayer was predicted to be stable with the semiconducting properties[14], and the  $\text{CrB}_4$  monolayer was predicted to be ferromagnetic with the Curie temperature of 401K[16]. Transition metal elements exhibit rich magnetic properties because of their unpaired electrons in  $d$ -orbitals. Despite the fact that the superconductivity have been predict to

---

\*morty.yu@yahoo.com

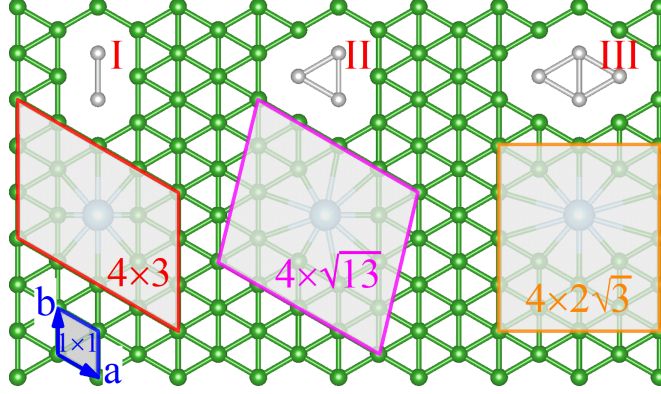


Figure 1: A schematic diagram of structure generation for monolayer titanium boride. A titanium atom substitutes two, three, and four boron atoms in type I, II, and III, respectively. The rhombus outlined by blue lines denotes the unitcell of 2D triangular lattice. Some supercells are also shown. The big sky-blue and small green spheres represent titanium and boron atoms, respectively. The gray spheres represent boron atoms to be substituted.

be exist in two-dimensional  $\text{Mo}_2\text{B}_2$ [1] and Li-decroated boron monolayers[32], the superconductivity is still out of sight in the transition metal boron monolayer.

Generally, the polymorphism of boron monolayers attribute to the variety of properties, but at the same time it become a challenge to screen the candidates due to the complicated potential energy surface[5]. Combined with the global optimization with the first-principles calculations, extensive researches have been focused on giving the concentration and distribution of vacancies in boron monolayers[34, 41], which might be synthesized on the certain metal surfaces. [46] In our previous studies, we used the motif of triangular lattice with hexagonal vacancies to construct possible borophenes which base on the inductive conclusion that when the number of boron atoms less than four, the borophene became less stable[38]. With this a prior knowledge, we explored all the structures through high-throughput first-principle calculation and the semiconducting monolayers were successfully predicted[36]. By using the similar strategy, the superconducting metal-boron monolayers are expected to be found based on the biased screening with proper motifs with the following two a prior knowledge a) transition metal and boron are were to form the stable planar clusters, b) the reported monolayer metal-boron materials were made up of hyper-coordinate metal-boron clusters and boron triangular grid fragments.

In the paper, an efficient method is proposed to construct  $\text{Ti@B}_n$  with the polygonal transition metal wheel motifs and triangular/quadrilateral boron motifs. Combining with the structue duplicate removal approach, we performed the high-throughput first-principles calculations on  $\text{TiB}_x$  ( $4 \leq x \leq 11$ ) monolayers, with the help of AiiDA [25] to maintain the reproducibility of the computational process. Besides  $\text{TiB}_4$  which is the same to the previously reported one, we predict two new stable monolayers of  $\text{TiB}_7$  and  $\text{TiB}_9$ . Notably, the  $\text{TiB}_7$  monolayer is found to be superconducting with the  $T_c$  of 8K.

## 2 Computational methods

In the recently proposed  $\text{TiB}_2$  sandwich structure[44], the vertical distance between titanium and boron network is 1.19 Å. Similar sandwich structure have also been predicted to be stable in titanium boride and iron boride. [37] Here our purpose is to search the stable monolayer transition boride. To form the monolayer transition metal boride, we need a boron network with transition metal embedded in. However, the transition metal such as titanium is too large to be embedded into the center of boron hexagonal ring to constructe the hexa-coordination motif. Therefore, hyper-coordination larger than six will be necessary for the creation of Ti-B monolayers. In order to sample the configurations efficiently in the phase space, we construct the possible candidates with specific motifs for the following reasons: a) stable boron monolayers are the triangular lattice with vacancies and transition metal atoms serve as the electrons donor; b) many hyper-coordinate transition boron clusters have been observed experimentally, which is considered to be the building blocks of the correspond monolayers.

The following steps were used to ergodically sample the configurations with the constrains mentioned above. First of all, the superlattice of boron lattice was created from extending the primitive of lattice which is shown in the Fig.1 (the blue quadrilateral in the left bottom corner). The unique deravative

superlattice with the unit cell sizes from 1 to 16 can be generated using Hermite Normal Form (HNF) matrices. [10] Each HNF matrix generates a superlattice of a size corresponding to its determinant  $n$  which is also the number of the boron atoms of the lattice. There exists many HNF matrices with the same determinant, each creating a variant superlattice. For example, the lattice in the Fig.1 are three lattice with different HNF matrices. Secondly, for each unique superlattice, we can substitute the two-body, three-body and four-body boron clusters by titanium atoms, where the type I, II and III correspond to the  $B_2$ ,  $B_3$  and  $B_4$  clusters are shown in the Fig.1. Finally, based on the structural recognition, we removed the duplicate configurations in order to prevent repeated computation.

The first-principles calculations were performed using the Vienna ab initio simulation package (VASP).[12] The projector-augmented plane wave (PAW) approach was used to represent the ion-electron interaction.[3, 13] The electron exchange-correlation functional was treated using generalized gradient approximation (GGA) in the form proposed by Perdew, Burke and Ernzerhof (PBE).[23] The energy cutoff of the plane wave was set to 350 eV. The Brillouin zone was sampled with allowed spacing between  $k$  points in  $0.2 \text{ \AA}^{-1}$ , with Monkhorst-Pack  $k$ -points grid for high-throughput geometry optimization. After high-throughput screening, the geometry optimization with high accuracy is performed for lowest ten structures in each composition. In this process, the atomic position were fully relaxed until the maximum force on each atom was less than  $10^{-2} \text{ eV/\AA}$ .

To study the superconductivity of  $TiB_x$ , the electron-phonon coupling (EPC) calculations were performed based on the density functional theory (DFT) and density functional perturbation theory (DFPT) implemented in QUANTUM-ESPRESSO package[9], employing the projector augmented-wave (PAW) pseudopotentials[3, 13] with Perdew-Burke-Ernzerhof (PBE) exchange-correlation energy functional [23]. The plane-wave cutoff energies for wavefunctions and charge density were set to 60 Ry and 600 Ry, respectively. A Marzari-Vanderbilt cold smearing [20] of 0.02 Ry was used for the corresponding electronic self-consistent cycles. Phonon frequencies and EPC parameter were calculated with a phonon wave-vector mesh of  $6 \times 6 \times 1$  and a dense  $k$  mesh of  $24 \times 24 \times 1$ , respectively.

Using Structures of Alloys Generation And Recognition (SAGAR) package[11], we have constructed the possible configurations up to the unit cell sizes up to 16 atoms, including 210, 98, 150 unique structures for type I, type II and type III substitution strategies respectively. During the high-throughput screening, the large number of simulations are involved and the complex sequence of logical steps are required in the study. To ensure reproducibility, we use AiiDA [25] as an open-source materials' informatics infrastructure to implement the calculation, keeping track of the full provenance of each calculation and results. All the calculation details is stored and exported to files which can be found in the materialcloud.

### 3 Results and discussion

Based on the the high-throughput first-principles calculations, we systematically investigate the structural stabilities of  $TiB_x$  ( $4 \leq x \leq 11$ ) monolayers in Section 3.1. The monolayers with superconductivity are discussed in Section 3.2, according to the electron-phonon coupling calculations.

#### 3.1 Structure stabilities of $TiB_x$ ( $4 \leq x \leq 11$ ) monolayers

Due to the remarkable difference of Ti-B and B-B bond lengths, titanium is considered to be unfavourably embedded in the 6-membered rings and forming hexa-coordinate wheels. In the recent study[26], the  $TiB_4$  monolayer was predicted to be a completely planar structure, in which B atoms form a network made up of 4-membered and 8-membered rings. Thus, the  $TiB_4$  monolayer was considered to be constructed with the motif of  $TiB_8$  wheels, where all titanium atoms were all embedded in the boron octagons.

As shown in Fig. 1, we introduce multi-vacancies (type I, II and III for the  $B_2$ ,  $B_3$  and  $B_4$  vacancies) in the boron triangular lattice, where the center of the vacancy is positioned with a single titanium atom. In such cases, titanium atoms are initially embedded in 8, 9, 10-membered rings, respectively. Based on the HNF matrices and structural recognition, we generated the possible candidates of  $TiB_x$  monolayers and the stable structures were further obtained through the structure relaxation.

To describe the stability of  $TiB_x$  monolayers, the formation enthalpy ( $\Delta H$ ) is calculated as:

$$\Delta H = (E_{TiB_x} - E_{Ti} - xE_B)/(1 + x) \quad (1)$$

, where  $E_{TiB_x}$ ,  $E_{Ti}$  and  $E_B$  are the total energies of one unit cell of the  $TiB_x$  monolayer, a single titanium atom in hexagonal close-packed (hcp) structure, a single boron atom in  $\alpha$ -borophene, respectively.

Fig.2(a) shows the  $\Delta H$  of  $Ti_xB_{1-x}$  as a function of titanium concentration. There are two  $TiB_4$  monolayers with lower formation energy, which are optimized from type I and III candidates. With

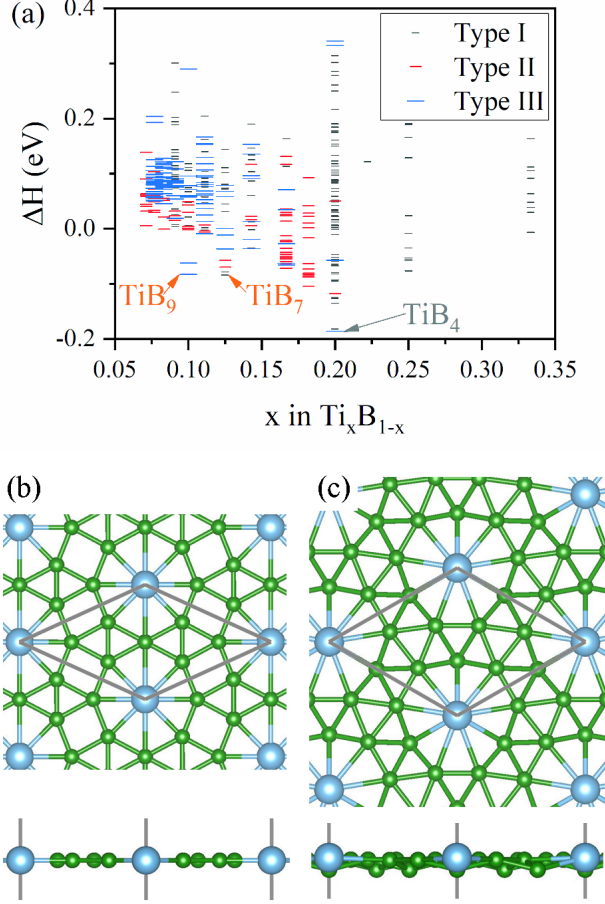


Figure 2: (a) The formation energy of monolayer titanium boride as a function of concentration ( $x$ ) of titanium. The top and side views of the atomic structure of predicted (b)  $\text{TiB}_7$  and (c)  $\text{TiB}_9$ .

titanium concentration higher than 0.2, the structures of type I are more stable, while type II and III candidates become more stable when the titanium concentration decrease.

Among the  $\text{TiB}_7$  structures, the one with lowest  $\Delta H$  (shown in Fig.2(b)) is completely flat. The relaxed lattice constants are  $a=5.72\text{\AA}$  and  $\gamma = 130.94^\circ$ . The spacegroup of the structure is Cmmm. In the structure, each titanium atom is octa-coordinated to boron atoms, the length of Ti-B bond are  $2.148\text{\AA}$ ,  $2.185\text{\AA}$  and  $2.373\text{\AA}$  respectively. The boron atoms forming a network composed of 3,4-membered rings connect to the  $\text{Ti@B}_8$  motif. For the most stable  $\text{TiB}_9$  (shown in Fig.2(c)), the relaxed lattice constants of the structure are  $a=5.83\text{\AA}$ ,  $\gamma = 120.0^\circ$ , with the spacegroup P31m. Each titanium atom is nona-coordinated to boron atoms, with the Ti-B bond length of  $2.216\text{\AA}$ ,  $2.432\text{\AA}$  and  $2.430\text{\AA}$  respectively. The boron atoms form a network composed of 3-membered rings connect to the  $\text{Ti@B}_9$  motif.

There are 14 different concentrations in the searching sub-space. Besides  $\text{TiB}_7$  and  $\text{TiB}_9$  as shown in the Fig.2, the most stable configurations of other concentrations are displayed in the ESI. We find that structures with either too high or too low titanium ratio are unstable. In the high titanium ratio conditions, titanium atoms tend to aggregate and the aggregations are then separated from the boron atoms. In the low titanium ratio configurations, boron atom forms a network structure. And because we didn't consider vacancies in constructing searching candidates, the low titanium structures here are necessarily no more stable than those with vacancies. We can also see from the stable structures of each concentration that  $\text{TiB}_4$ ,  $\text{TiB}_7$ ,  $\text{Ti}_2\text{B}_9$  and  $\text{TiB}_5$  are totally flat monolayer also known as real two-dimensional structures such as graphene and borophene. In order to forming such kinds of novel structure, the electronic charge need to be avaragely distributed between titanium and borons which require the ratio of titaniums restricted in the suitable range.

Fig.3 show the electronic properties of the  $\text{TiB}_7$  and  $\text{TiB}_9$  monolayers, including the projected density of states(PDOS) and band structures. Both the  $\text{TiB}_7$  and  $\text{TiB}_9$  monolayers are metal due to the bands across the Fermi level, which are mainly attributed by the Ti- $d$  states. Comparing to the  $\text{TiB}_4$

monolayer[26], the  $d$  states in these monolayers provide a similar flat band, which increases the density of states near the Fermi level effectively, indicating the possible superconductivity.

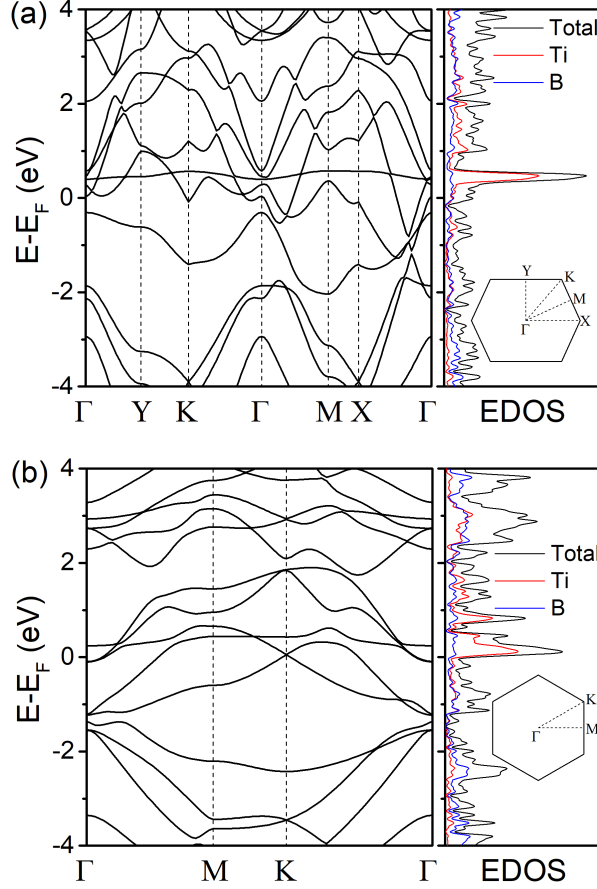


Figure 3: The band structures and electronic density of states of (a) TiB<sub>7</sub> and (b) TiB<sub>9</sub>. The first Brillouin zones are shown in the inset.

### 3.2 Superconductivity of TiB<sub>7</sub> and TiB<sub>9</sub> monolayers

To consider the possible superconductivity, we further studied electron-phonon coupling (EPC) in the TiB<sub>7</sub> monolayer. The dynamic stability of TiB<sub>7</sub> was inferred from the phonon spectra without imaginary frequency (see Fig. 4a). The EPC constant  $\lambda$  was a dimensionless measurement of Eliashberg spectral function  $\alpha^2F(\omega)$ ,

$$\lambda = 2 \int \frac{\alpha^2F(\omega)}{\omega} d\omega. \quad (2)$$

The  $\alpha^2F(\omega)$  was calculated with following equation,

$$\alpha^2F(\omega) = \frac{1}{2\pi N(E_F)} \sum_{qv} \delta(\omega - \omega_{qv}) \frac{\gamma_{qv}}{\hbar\omega_{qv}}. \quad (3)$$

where  $N(E_F)$  is the electronic density of states at the Fermi level, and the Dirac  $\delta$  function is simulated by a Gaussian function.  $\gamma_{qv}$  is the linewidth of phonon mode  $v$  at wave vector  $q$ .

The phonon dispersions with phonon linewidth  $\gamma_{qv}$ , phonon density of states (PHDOS), Eliashberg function  $\alpha^2F(\omega)$ , and  $\lambda(\omega)$  of monolayer TiB<sub>7</sub> are shown in Fig. 4a. The low frequency modes ( $< 400\text{cm}^{-1}$ ) induce the main EPC. There is a peak at the frequency of  $200\text{cm}^{-1}$  in Eliashberg function  $\alpha^2F(\omega)$ . The vibrational modes at  $\Gamma$  with the frequencies of around  $200\text{cm}^{-1}$  have large phonon linewidth. Fig. 2b shows a larger view of phonon dispersions with phonon linewidth around  $\Gamma$  point with

the frequencies ranging from  $160$  to  $240\text{cm}^{-1}$ . The shear mode shown in Fig. 4c has a  $C_3$  rotation operation. These layer breathing modes shown in Fig. 4d, 4e, and 4f contain roto-reflection, rotational, and mirror symmetry, respectively. The shear and layer breathing modes represent the vibrations perpendicular and parallel to normal[45]. The shear mode with a frequency of  $185\text{cm}^{-1}$  and the layer breathing modes with frequencies of  $212$  and  $217\text{cm}^{-1}$  have large phonon linewidth. The phonon linewidth of the layer breathing mode at  $\Gamma$  point with the frequency of  $204\text{cm}^{-1}$  is smaller than those of mentioned three modes, but the phonon branch including this mode is fairly flat around  $\Gamma$  point. As a result, a peak appears at the frequency of  $200\text{cm}^{-1}$  in Eliashberg function  $\alpha^2F(\omega)$ . Meanwhile the mentioned four modes are caused by the vibrations of boron atoms.

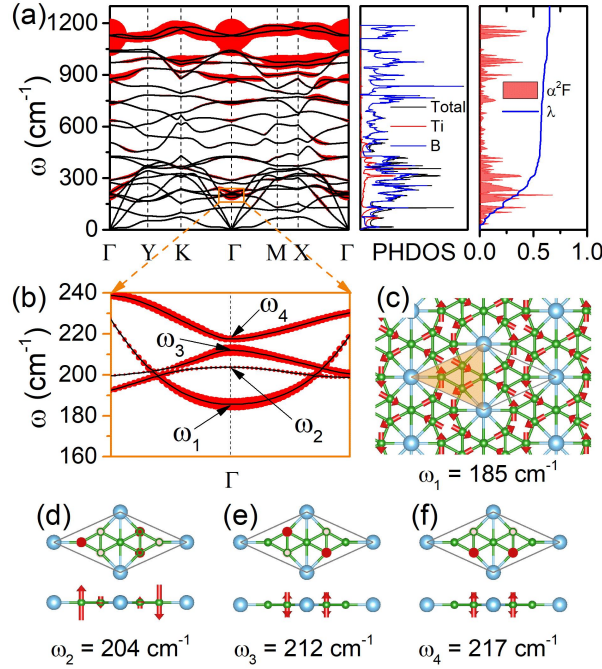


Figure 4: (a) Phonon dispersions with phonon linewidth  $\gamma_{qv}$  in red bubble, phonon density of states and Eliashberg function  $\alpha^2F(\omega)$  with  $\lambda(\omega)$  of monolayer  $\text{TiB}_7$ . (b) A larger view of the rectangular area in (a). (c) A shear mode at  $\Gamma$ . The filled triangle covers exactly half of a unitcell. (d-f) Some layer breathing modes. The red arrows and their lengths represent the directions and amplitudes of the corresponding vibrational modes.

We estimate superconducting transition temperature ( $T_c$ ) by using the McMillan-Allen-Dynes parameterized Eliashberg equation [2],

$$T_c = \frac{\omega_{\log}}{1.2} \exp \left( -\frac{1.04(1 + \lambda)}{\lambda - \mu^*(1 + 0.62\lambda)} \right), \quad (4)$$

where  $\omega_{\log}$  is the logarithmic averaged phonon frequency

$$\omega_{\log} = \exp \left( \frac{2}{\lambda} \int \frac{\alpha^2F(\omega) \log(\omega)}{\omega} d\omega \right). \quad (5)$$

Following the previous studies on superconductivity in boron-base materials [17, 22, 39, 48, 49], we use the Coulomb repulsion pseudopotential  $\mu^* = 0.1$  to calculate the transition temperature. The estimated  $T_c$  of unstrained monolayer  $\text{TiB}_7$  reaches  $8.3\text{K}$  with  $\lambda$  equals to  $0.65$ . In the most stable  $\text{B}_8$  sheet ( $\alpha$ -sheet,  $\eta = 1/9$  [30, 40]), the  $T_c$  is  $3.7\text{K}$  and with  $\lambda = 0.52$ . In the  $\text{B}_7$  sheet ( $\eta = 1/8$ ), the  $T_c$  and  $\lambda$

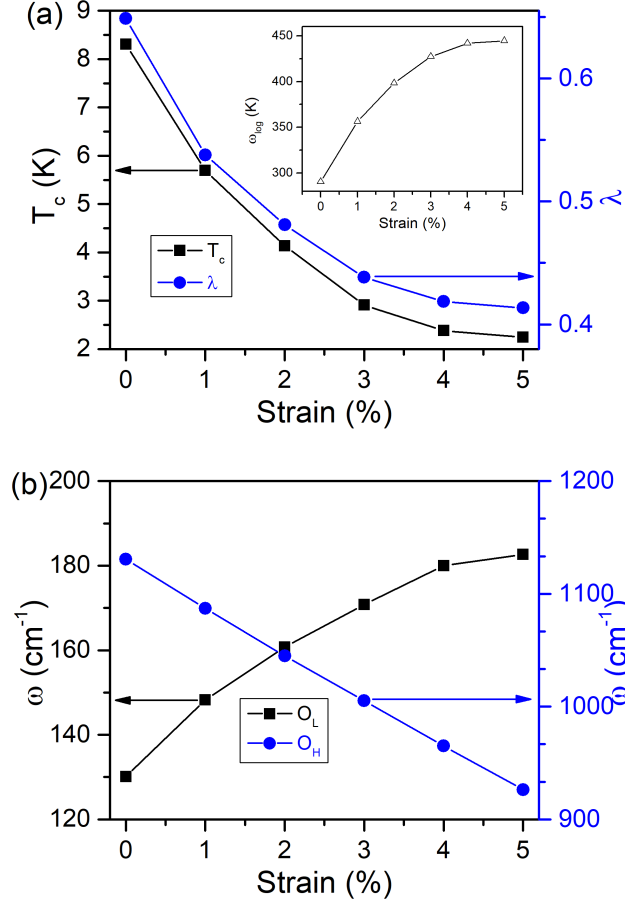


Figure 5: (a) Calculated superconducting transition temperature ( $T_c$ ) and electron-phonon coupling constant ( $\lambda$ ) of monolayer  $\text{TiB}_7$  as a function of equibiaxial tensile strain. The evolution of the logarithmic averaged phonon frequency ( $\omega_{\log}$ ) is shown in the inset. (b) The lowest ( $O_L$ ) and highest ( $O_H$ ) frequencies of optical phonons at  $\Gamma$  as a function of strain.

increase to 5.8 K and 0.58, respectively [48]. So the introduction of titanium atom in  $\text{B}_7$  sheet strengthens the electron-phonon coupling and enlarges the transition temperature  $T_c$ . The two-dimensional  $\text{AlB}_6$  is reported to be an intrinsic BCS-type superconductor and the  $T_c$  is predicted to be greatly enhanced to 30 K by a equibiaxial tensile strain of 12% [29]. However, the superconductivity in monolayer  $\text{TiB}_7$  is significantly suppressed by tensile strain, as shown in Fig. 5a. The  $T_c$  and  $\lambda$  decrease in unison even though the  $\omega_{\log}$  increases in sequence. The frequencies of low frequency phonons increase by tensile strain, and the frequencies of high frequency phonons decrease gradually. Fig. 5b shows the lowest ( $O_L$ ) and highest ( $O_H$ ) frequencies of optical phonons at  $\Gamma$  as a function of strain. The details of the evolution of phonon spectra are shown in Fig. S1. Phonon-mediated superconductivity of  $\text{B}_5$  sheet ( $\beta_{12}$ ,  $\eta = 1/6$ ) is also suppressed by tensile strain [4]. In addition, a previous experiment showed that tensile strain suppresses superconductivity in FeSe films [21]. Generally, if the tensile strain suppresses the superconductivity of a material, the compressive strain would enhance it, and vice versa, such as the triangular boron monolayer without vacancy ( $\delta_6$ ,  $\eta = 1/6$ ) [35] and two dimensional  $\text{TiS}_2$  [18]. So we expected the compressive strain could enhance the superconductivity of monolayer  $\text{TiB}_7$ . However, imaginary frequencies appear in the phonon spectra when applying the compressive strain of 1% (see Fig. S2).

For comparison, we have also studied the  $\text{TiB}_9$  monolayer, for which there is no imaginary frequency in the phonon spectra (see Fig. S3). The EPC calculation shows a small  $\lambda$  of 0.40. The  $T_c$  is predicted to be 1.22 K. With smaller  $\lambda$  of 0.10 and 0.27, the recently proposed two dimensional  $\text{TiB}_2$  [44] and  $\text{Ti}_2\text{B}_2$  [31] are not superconductors because of too weak electron-phonon coupling. The most stable monolayer  $\text{TiB}_4$ , a completely planar structure [26], is also not superconducting due to a small  $\lambda$  of 0.18.



## Conclusions

In summary, we have theoretically investigated a series of planar two dimensional structures of  $\text{TiB}_x$  ( $4 \leq x \leq 11$ ) through high-throughput first-principles calculations. We successfully predicted a superconducting metal-boron monolayer of  $\text{TiB}_7$  at the first time, where the  $T_c$  is as high as 8K. A new structure of  $\text{TiB}_9$  was also found to be a thermodynamic stable monolayer. In our study, the transition metal monolayers are generated with reasonable motifs which can be summarized as a new approach to quickly search target structures under certain a prior structure constraints. Consequently, the motif based search strategy can be extended and used to explore the new materials with specific structure pattern.

## Conflicts of interest

There are no conflicts to declare.

**Acknowledgements** This work was supported by Guangdong Natural Science Funds for Distinguished Young Scholars (No. 2014A030306024) and for Doctoral Program (Grant No. 2017A030310086), National Natural Science Foundation of China (No. 11474100, U1601212), the Fundamental Research Funds for the Central Universities(No. 2018ZD46).

## References

- [1] Prediction of phonon-mediated superconductivity in two-dimensional  $\text{Mo}_2\text{B}_2$ . *Journal of Materials Chemistry C*, 7(9):2589–2595, 2019. ISSN 20507526. doi:10.1039/c8tc06123h.
- [2] P. B. Allen and R. C. Dynes. Transition temperature of strong-coupled superconductors reanalyzed. *Physical Review B*, 12:905–922, Aug 1975. doi:10.1103/PhysRevB.12.905. URL <https://link.aps.org/doi/10.1103/PhysRevB.12.905>.
- [3] P. E. Blöchl. Projector augmented-wave method. *Physical Review B*, 50:17953–17979, Dec 1994. doi:10.1103/PhysRevB.50.17953. URL <https://link.aps.org/doi/10.1103/PhysRevB.50.17953>.
- [4] Cai Cheng, Jia-Tao Sun, Hang Liu, Hui-Xia Fu, Jin Zhang, Xiang-Rong Chen, and Sheng Meng. Suppressed superconductivity in substrate-supported  $\beta$  12 borophene by tensile strain and electron doping. *2D Materials*, 4(2):025032, 2017.
- [5] Sandip De, Alexander Willand, Maximilian Amsler, Pascal Pochet, Luigi Genovese, and Stefan Goedecker. Energy landscape of fullerene materials: A comparison of boron to boron nitride and carbon. *Physical review letters*, 106:225502, Jun 2011. doi:10.1103/PhysRevLett.106.225502. URL <https://link.aps.org/doi/10.1103/PhysRevLett.106.225502>.
- [6] Baojie Feng, Jin Zhang, Qing Zhong, Wenbin Li, Shuai Li, Hui Li, Peng Cheng, Sheng Meng, Lan Chen, and Kehui Wu. Experimental realization of two-dimensional boron sheets. *Nature Chemistry*, 8(6):563–568, Jun 2016. ISSN 17554349. doi:10.1038/nchem.2491.
- [7] Baojie Feng, Osamu Sugino, Ro-Ya Liu, Jin Zhang, Ryu Yukawa, Mitsuaki Kawamura, Takushi Iimori, Howon Kim, Yukio Hasegawa, Hui Li, Lan Chen, Kehui Wu, Hiroshi Kumigashira, Fumio Komori, Tai-Chang Chiang, Sheng Meng, and Iwao Matsuda. Dirac fermions in borophene. *Physical review letters*, 118:096401, Mar 2017. doi:10.1103/PhysRevLett.118.096401. URL <https://link.aps.org/doi/10.1103/PhysRevLett.118.096401>.
- [8] M. Fujimori, T. Nakata, T. Nakayama, E. Nishibori, K. Kimura, M. Takata, and M. Sakata. Peculiar Covalent Bonds in  $\alpha$ -Rhombohedral Boron. *Physical review letters*, 82(22):4452–4455, 1999. ISSN 10797114. doi:10.1103/PhysRevLett.82.4452.
- [9] Paolo Giannozzi, Stefano Baroni, Nicola Bonini, Matteo Calandra, Roberto Car, Carlo Cavazzoni, Davide Ceresoli, Guido L. Chiarotti, Matteo Cococcioni, Ismaila Dabo, Andrea Dal Corso, Stefano De Gironcoli, Stefano Fabris, Guido Fratesi, Ralph Gebauer, Uwe Gerstmann, Christos Gougoussis, Anton Kokalj, Michele Lazzeri, Layla Martin-Samos, Nicola Marzari, Francesco Mauri, Riccardo



- Mazzarello, Stefano Paolini, Alfredo Pasquarello, Lorenzo Paulatto, Carlo Sbraccia, Sandro Scandolo, Gabriele Sciauzero, Ari P. Seitsonen, Alexander Smogunov, Paolo Umari, and Renata M. Wentzcovitch. QUANTUM ESPRESSO: A modular and open-source software project for quantum simulations of materials. *Journal of Physics Condensed Matter*, 21(39), 2009. ISSN 09538984. doi:10.1088/0953-8984/21/39/395502. arXiv:0906.2569.
- [10] Gus L. W. Hart and Rodney W. Forcade. Algorithm for generating derivative structures. *Physical Review B*, 77:224115, Jun 2008. doi:10.1103/PhysRevB.77.224115. URL <https://link.aps.org/doi/10.1103/PhysRevB.77.224115>.
  - [11] Yu Jason and He ChangChun. Structures of alloy generation and recognition. <https://github.com/scut-ccmp/sagar>, 2019.
  - [12] G. Kresse and J. Furthmüller. Efficient iterative schemes for ab initio total-energy calculations using a plane-wave basis set. *Physical Review B*, 54:11169–11186, Oct 1996. doi:10.1103/PhysRevB.54.11169. URL <https://link.aps.org/doi/10.1103/PhysRevB.54.11169>.
  - [13] G. Kresse and D. Joubert. From ultrasoft pseudopotentials to the projector augmented-wave method. *Physical Review B*, 59:1758–1775, Jan 1999. doi:10.1103/PhysRevB.59.1758. URL <https://link.aps.org/doi/10.1103/PhysRevB.59.1758>.
  - [14] Jiao Li, Yanpei Wei, Xinyu Fan, Hongbo Wang, Yang Song, Gang Chen, Yunye Liang, Vei Wang, and Yoshiyuki Kawazoe. Global minimum of two-dimensional FeB6 and an oxidization induced negative Poisson’s ratio: A new stable allotrope. *Journal of Materials Chemistry C*, 4(40):9613–9621, oct 2016. ISSN 20507526. doi:10.1039/c6tc03710k.
  - [15] Wei-Li Li, Ya-Fan Zhao, Han-Shi Hu, Jun Li, and Lai-Sheng Wang. b30: A quasiplanar chiral boron cluster. *Angewandte Chemie International Edition*, 53(22):5540–5545, 2014. doi:10.1002/anie.201402488. <https://onlinelibrary.wiley.com/doi/pdf/10.1002/anie.201402488>. URL <https://onlinelibrary.wiley.com/doi/abs/10.1002/anie.201402488>.
  - [16] Xiangyang Li, Xingxing Li, and Jinlong Yang. Room-Temperature Ferromagnetism in Transition Metal Embedded Borophene Nanosheets. *The Journal of Physical Chemistry Letters*, 10(15):4417–4421, aug 2019. ISSN 1948-7185. doi:10.1021/acs.jpclett.9b01667. URL <https://pubs.acs.org/doi/10.1021/acs.jpclett.9b01667>.
  - [17] Ji Hai Liao, Yin Chang Zhao, Yu Jun Zhao, Hu Xu, and Xiao Bao Yang. Phonon-mediated superconductivity in Mg intercalated bilayer borophenes. *Physical Chemistry Chemical Physics*, 19(43):29237–29243, 2017. ISSN 14639076. doi:10.1039/c7cp06180c.
  - [18] Ji-Hai Liao, Yin-Chang Zhao, Yu-Jun Zhao, Xiao-Bao Yang, and Yue Chen. Doping induced charge density wave in monolayer  $\text{TiS}_2$  and phonon-mediated superconductivity. *Journal of Applied Physics*, 127(4):044301, 2020.
  - [19] Xiaolong Liu, Zhuhua Zhang, Luqing Wang, Boris I. Yakobson, and Mark C. Hersam. Intermixing and periodic self-assembly of borophene line defects, sep 2018. ISSN 14764660.
  - [20] Nicola Marzari, David Vanderbilt, Alessandro De Vita, and M. C. Payne. Thermal contraction and disordering of the  $\text{Al}(110)$  surface. *Physical review letters*, 82:3296–3299, Apr 1999. doi:10.1103/PhysRevLett.82.3296. URL <https://link.aps.org/doi/10.1103/PhysRevLett.82.3296>.
  - [21] YF Nie, E Brahimi, JI Budnick, WA Hines, M Jain, and BO Wells. Suppression of superconductivity in fese films under tensile strain. *Applied Physics Letters*, 94(24):242505, 2009.
  - [22] Evgeni S. Penev, Alex Kutana, and Boris I. Yakobson. Can Two-Dimensional Boron Superconduct? *Nano Letters*, 16(4):2522–2526, apr 2016. ISSN 1530-6984. doi:10.1021/acs.nanolett.6b00070. URL <https://pubs.acs.org/doi/10.1021/acs.nanolett.6b00070>.
  - [23] John P. Perdew, Kieron Burke, and Matthias Ernzerhof. Generalized gradient approximation made simple. *Physical review letters*, 77:3865–3868, Oct 1996. doi:10.1103/PhysRevLett.77.3865. URL <https://link.aps.org/doi/10.1103/PhysRevLett.77.3865>.

- [24] Zachary A. Piazza, Han Shi Hu, Wei Li Li, Ya Fan Zhao, Jun Li, and Lai Sheng Wang. Planar hexagonal B 36 as a potential basis for extended single-atom layer boron sheets. *Nature Communications*, 5:5113, jan 2014. ISSN 20411723. doi:10.1038/ncomms4113.
- [25] Giovanni Pizzi, Andrea Cepellotti, Riccardo Sabatini, Nicola Marzari, and Boris Kozinsky. AiIDA: automated interactive infrastructure and database for computational science. *Computational Materials Science*, 111:218–230, 2016. ISSN 09270256. doi:10.1016/j.commatsci.2015.09.013. arXiv:1504.01163. URL <http://dx.doi.org/10.1016/j.commatsci.2015.09.013>.
- [26] Xin Qu, Jinghai Yang, Yanchao Wang, Jian Lv, Zhongfang Chen, and Yanming Ma. A two-dimensional tib 4 monolayer exhibits planar octacoordinate ti. *Nanoscale*, 9(45):17983–17990, 2017.
- [27] Constantin Romanescu, Timur R. Galeev, Wei-Li Li, Alexander I. Boldyrev, and Lai-Sheng Wang. Aromatic Metal-Centered Monocyclic Boron Rings: CoB8 and RuB9. *Angewandte Chemie International Edition*, 50(40):9334–9337, sep 2011. ISSN 14337851. doi:10.1002/anie.201104166. URL <http://doi.wiley.com/10.1002/anie.201104166>.
- [28] J. W. Simonson, D. Wu, S. J. Poon, and S. A. Wolf. Superconductivity in transition metal doped MoB 4. *Journal of Superconductivity and Novel Magnetism*, 23(3):417–422, apr 2010. ISSN 15571939. doi:10.1007/s10948-009-0593-3.
- [29] Bingyi Song, Yuan Zhou, Hui-Min Yang, Ji-Hai Liao, Li-Ming Yang, Xiao-Bao Yang, and Eric Ganz. Two-Dimensional Anti-Van’t Hoff/Le Bel Array AIB  $\langle \text{sub} \rangle 6 \langle \text{sub} \rangle$  with High Stability, Unique Motif, Triple Dirac Cones, and Superconductivity. *Journal of the American Chemical Society*, 141(8):3630–3640, feb 2019. ISSN 0002-7863. doi:10.1021/jacs.8b13075. URL <https://pubs.acs.org/doi/10.1021/jacs.8b13075>.
- [30] Hui Tang and Sohrab Ismail-Beigi. Novel precursors for boron nanotubes: The competition of two-center and three-center bonding in boron sheets. *Physical review letters*, 99:115501, Sep 2007. doi:10.1103/PhysRevLett.99.115501. URL <https://link.aps.org/doi/10.1103/PhysRevLett.99.115501>.
- [31] Junjie Wang, Tian-Nan Ye, Yutong Gong, Jiazhen Wu, Nanxi Miao, Tomofumi Tada, and Hideo Hosono. Discovery of hexagonal ternary phase ti 2 inb 2 and its evolution to layered boride tib. *Nature communications*, 10(1):1–8, 2019.
- [32] Chao Wu, Hua Wang, Jiajia Zhang, Gaoyang Gou, Bica Pan, and Ju Li. Lithium–Boron (Li–B) Monolayers: First-Principles Cluster Expansion and Possible Two-Dimensional Superconductivity. *ACS Applied Materials & Interfaces*, 8(4):2526–2532, feb 2016. ISSN 1944-8244. doi:10.1021/acsami.5b09949. URL <https://pubs.acs.org/doi/10.1021/acsami.5b09949>.
- [33] Rongting Wu, Ilya K. Drozdov, Stephen Eltinge, Percy Zahl, Sohrab Ismail-Beigi, Ivan Božović, and Adrian Gozar. Large-area single-crystal sheets of borophene on Cu(111) surfaces, jan 2019. ISSN 17483395.
- [34] Xiaojun Wu, Jun Dai, Yu Zhao, Zhiwen Zhuo, Jinlong Yang, and Xiao Cheng Zeng. Two-Dimensional Boron Monolayer Sheets. *ACS Nano*, 6(8):7443–7453, aug 2012. ISSN 1936-0851. doi:10.1021/nn302696v. URL <https://pubs.acs.org/doi/10.1021/nn302696v>.
- [35] RC Xiao, DF Shao, WJ Lu, HY Lv, JY Li, and YP Sun. Enhanced superconductivity by strain and carrier-doping in borophene: A first principles prediction. *Applied Physics Letters*, 109(12):122604, 2016.
- [36] Shao-Gang Xu, Xiao-Tian Li, Yu-Jun Zhao, Ji-Hai Liao, Wang-Ping Xu, Xiao-Bao Yang, and Hu Xu. Two-Dimensional Semiconducting Boron Monolayers. *Journal of the American Chemical Society*, 139(48):17233–17236, dec 2017. ISSN 0002-7863. doi:10.1021/jacs.7b08680. URL <https://pubs.acs.org/doi/10.1021/jacs.7b08680>.
- [37] Shao Gang Xu, Yu Jun Zhao, Xiao Bao Yang, and Hu Xu. Stable sandwich structures of two-dimensional iron borides FeBX alloy: A first-principles calculation. *RSC Advances*, 7(48):30320–30326, jun 2017. ISSN 20462069. doi:10.1039/c7ra03153j.

- [38] Shao Gang Xu, Xiao Tian Li, Yu Jun Zhao, Ji Hai Liao, Hu Xu, and Xiao Bao Yang. An electron compensation mechanism for the polymorphism of boron monolayers. *Nanoscale*, 10(28):13410–13416, jul 2018. ISSN 20403372. doi:10.1039/c8nr01230j.
- [39] Luo Yan, Tao Bo, Peng-Fei Liu, Liujiang Zhou, Junrong Zhang, Ming-Hua Tang, Yong-Guang Xiao, and Bao-Tian Wang. Superconductivity in predicted two dimensional XB 6 (X = Ga, In) . *Journal of Materials Chemistry C*, 8:1704–1714, 2020. ISSN 2050-7526. doi:10.1039/c9tc05783h.
- [40] Xiaobao Yang, Yi Ding, and Jun Ni. Ab initio prediction of stable boron sheets and boron nanotubes: Structure, stability, and electronic properties. *Physical Review B*, 77(4):041402, jan 2008. ISSN 10980121. doi:10.1103/PhysRevB.77.041402.
- [41] Xiao Yu, Lanlan Li, Xue-Wen Xu, and Cheng-Chun Tang. Prediction of Two-Dimensional Boron Sheets by Particle Swarm Optimization Algorithm. *The Journal of Physical Chemistry C*, 116(37):20075–20079, sep 2012. ISSN 1932-7447. doi:10.1021/jp305545z. URL <https://pubs.acs.org/doi/10.1021/jp305545z>.
- [42] Hua Jin Zhai, Boggavarapu Kiran, Jun Li, and Lai Sheng Wang. Hydrocarbon analogues of boron clusters planarity, aromaticity and antiaromaticity. *Nature Materials*, 2(12):827–833, 2003. ISSN 14761122. doi:10.1038/nmat1012.
- [43] Haijun Zhang, Yafei Li, Jianhua Hou, Kaixiong Tu, and Zhongfang Chen. FeB <sub>6</sub> Monolayers: The Graphene-like Material with Hypercoordinate Transition Metal. *Journal of the American Chemical Society*, 138(17):5644–5651, may 2016. ISSN 0002-7863. doi:10.1021/jacs.6b01769. URL <https://pubs.acs.org/doi/10.1021/jacs.6b01769>.
- [44] L. Z. Zhang, Z. F. Wang, S. X. Du, H.-J. Gao, and Feng Liu. Prediction of a dirac state in monolayer tib<sub>2</sub>. *Physical Review B*, 90:161402, Oct 2014. doi:10.1103/PhysRevB.90.161402. URL <https://link.aps.org/doi/10.1103/PhysRevB.90.161402>.
- [45] X. Zhang, W. P. Han, J. B. Wu, S. Milana, Y. Lu, Q. Q. Li, A. C. Ferrari, and P. H. Tan. Raman spectroscopy of shear and layer breathing modes in multilayer mos<sub>2</sub>. *Physical Review B*, 87:115413, Mar 2013. doi:10.1103/PhysRevB.87.115413. URL <https://link.aps.org/doi/10.1103/PhysRevB.87.115413>.
- [46] Zhuhua Zhang, Yang Yang, Guoying Gao, and Boris I. Yakobson. Two-Dimensional Boron Monolayers Mediated by Metal Substrates. *Angewandte Chemie International Edition*, 54(44):13022–13026, oct 2015. ISSN 14337851. doi:10.1002/anie.201505425. URL <http://doi.wiley.com/10.1002/anie.201505425>.
- [47] Zhuhua Zhang, Andrew J Mannix, Xiaolong Liu, Zhili Hu, Nathan P Guisinger, Mark C Hersam, and Boris I Yakobson. Near-equilibrium growth from borophene edges on silver. Technical Report 9, 2019.
- [48] Yinchang Zhao, Shuming Zeng, and Jun Ni. Phonon-mediated superconductivity in borophenes. *Applied Physics Letters*, 108(24):242601, jun 2016. ISSN 00036951. doi:10.1063/1.4953775.
- [49] Yinchang Zhao, Shuming Zeng, Chao Lian, Zhenhong Dai, Sheng Meng, and Jun Ni. Multigap anisotropic superconductivity in borophenes. *Physical Review B*, 98:134514, Oct 2018. doi:10.1103/PhysRevB.98.134514. URL <https://link.aps.org/doi/10.1103/PhysRevB.98.134514>.